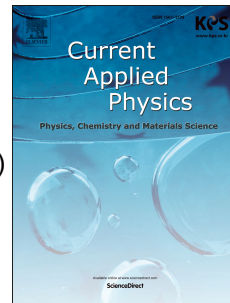


Accepted Manuscript

Stress relaxation and transitions in optical bandgap of yttrium doped zinc oxide (YZO) thin films

Narinder Kaur, Sanjeev K. Sharma, Deuk Young kim



PII: S1567-1739(15)30132-2

DOI: [10.1016/j.cap.2015.12.004](https://doi.org/10.1016/j.cap.2015.12.004)

Reference: CAP 4128

To appear in: *Current Applied Physics*

Received Date: 3 August 2015

Revised Date: 25 November 2015

Accepted Date: 6 December 2015

Please cite this article as: N. Kaur, S.K. Sharma, D. Young kim, Stress relaxation and transitions in optical bandgap of yttrium doped zinc oxide (YZO) thin films, *Current Applied Physics* (2016), doi: [10.1016/j.cap.2015.12.004](https://doi.org/10.1016/j.cap.2015.12.004).

This is a PDF file of an unedited manuscript that has been accepted for publication. As a service to our customers we are providing this early version of the manuscript. The manuscript will undergo copyediting, typesetting, and review of the resulting proof before it is published in its final form. Please note that during the production process errors may be discovered which could affect the content, and all legal disclaimers that apply to the journal pertain.

Stress relaxation and transitions in optical bandgap of yttrium doped zinc oxide (YZO) thin films

Narinder Kaur, Sanjeev K. Sharma*, Deuk Young kim*

Semiconductor Materials and Device Laboratory, Department of Semiconductor Science,
Dongguk University-Seoul, Jung-gu, Seoul 100715, Republic of Korea

*Corresponding Author: sksharma@dongguk.edu, dykim@dongguk.edu, Fax:+82-2-2260-3945

ABSTRACT

The stress relaxation and its effect on the bandgap of Y-doped ZnO (YZO) thin films were investigated by thermal annealing. YZO thin films were prepared on quartz glass by spin coating and subsequent annealed in vacuum. All the annealed YZO films showed a preferred (002) orientation. Photoluminescence (PL) provides the direct evidence of shifting the bandgap owing to stress release phenomena. The shifting in bandgap by increasing the annealing temperature can be attributed to the stress relaxation of YZO thin films. The bandgap of annealed films was initially decreased due to increase in magnitude of compressive stress and then increased as the tensile stress induced in the films. Therefore, these results may suggest the way to tune the band gap of YZO thin films by varying the residual stress through annealing.

Keywords: YZO thin films, sol-gel deposition and thermal annealing, microstructural analysis, stress relaxation, optical parameters

1. INTRODUCTION

ZnO is one of the most versatile and promising materials due to its large bandgap (3.37 eV) and high exciton binding energy (60 meV) at room temperature (RT) which makes it more attractive for the development of optoelectronic devices [1-3]. Moreover, the performance of these devices are strongly dependent on the quality of ZnO thin films. Since cost effectiveness is an important issue in the practical applications of ZnO films, it is attractive to develop a simple and the effective process to further reduce the fabrication cost. Various deposition methods, such as sputtering [4-6], spray pyrolysis [7], pulse laser deposition [8, 9], chemical vapor deposition [10], and sol-gel process [11, 12], have been used to produce ZnO thin films. Among them, sol-gel process is one of the least expensive, simple, and non-vacuum deposition methods that enable to produce a large area of thin films.

In recent time, the research has been focused to improve the physical properties of transparent ZnO thin films with an addition of rare earth dopants [13-16]. Based on the prior literature survey, it has been found that yttrium, Y, has become one of the most appropriate choice as n-type dopant of ZnO for highly transparent thin films [17] for the detection of antibacterial activity [18] and gas sensors [19]. Annealing is one of the controlling parameters of ZnO thin films that manipulates the physical properties [20]. Yu et al. [21] investigated the annealing effect on YZO thin films and observed a significant influence on the surface morphology and absence of green emission at room temperature PL. Annealing and dopant concentrations can also affect the residual stress, crystal structure, optical and electrical properties of ZnO thin films [22]. Lately, Heo et al. [23] investigated the residual stress and the crystal structure of nanostructured YZO, which were dependent on the mole concentration. Malek et al. [24] observed the stress relaxation in ZnO thin films grown on glass and annealed at

500 °C. Li et al. [25] proposed the relationship between bandgap and the residual stress in ZnO thin films by combining the experimental results with the first principle calculation. There are several reports indicated that the annealing of ZnO thin films can control the residual stress, which affects the physical and electrical properties [26-28]. Thus, it is extensively important to understand the residual stress of YZO thin films and its impact on the physical properties. Some other factors such as lattice mismatch with the substrate and/or at the interface of layers, post annealing process is responsible for the releasing of the residual stress or stress relaxation in thin films [29-32]. So far, the residual stress of nanostructured YZO thin films and its impact on the physical properties are poorly understood. Nevertheless, it is required to study the extensive annealing effect on the YZO thin films for the evaluation of the residual stress and its influence on the physical properties. Reports are scarcely available, which deals with bandgap fluctuations with stress generated and/or released due to annealing of YZO thin films.

In this work, we synthesized YZO (Y: 2 at.%) thin films on quartz glass substrates by using sol-gel method and subsequent annealed at 400 - 700 °C in vacuum. This report reveals the variation of bandgap and the release in stresses by thermal annealing for better understanding and to improve the quality of YZO thin films.

II. EXPERIMENT

YZO (Y: 2 at.%) thin films were deposited on quartz glass substrates by spin coating. The sol was prepared by dissolving 0.5 M zinc acetate dehydrate ($\text{Zn}(\text{CH}_3\text{COO})_2 \cdot 2\text{H}_2\text{O}$) in 2-methoxy-ethanol ($\text{C}_3\text{H}_8\text{O}_2$) at room temperature (RT) and mixed with a magnetic stirrer at 60 °C for 2 h. Yttrium acetate hydrate ($\text{Y}(\text{CH}_3\text{COO})_2 \cdot \text{H}_2\text{O}$) was used as a dopant concentration. To yield a transparent and clear solution, a stabilizing agent, monoethanolamine (MEA) was added

drop-by-drop. To obtain optimal viscosity, the solution was aged for 24 h. The prepared solution was spin coated on the ultrasonically cleaned quartz glass substrates and dried at 300 °C for 10 min to remove the organic residues. The coating procedure was repeated up to 10 cycles to attain the suitable thickness. In order to investigate the influence of annealing temperature on the physical properties, YZO thin films were annealed at different temperatures (400~700°C) in vacuum by using the rapid thermal annealing (RTA) system. The surface morphology of YZO thin films were examined by field emission-scanning electron microscopy (FE-SEM) (Hitachi-S-4700). The crystallographic orientation of the films were investigated by x-ray diffraction (XRD) using Cu $K\alpha_1$ ($\lambda=0.154$ nm) radiation. The bandgap of YZO thin films were calculated from their respective transmission spectra recorded by using UV-visible spectrophotometer (WFZ-26). The photoluminescence (PL) was measured at room temperature by the excitation laser (He-Cd) of wavelength 325 nm.

III. RESULTS AND DISCUSSION

Fig. 1 (a) shows the XRD patterns of as-deposited and annealed YZO (2 at.%) thin films.

All YZO thin films showed the polycrystalline behavior with the hexagonal wurtzite structure having preferential (002) orientation. In-order-to investigate the effect of annealing temperature on the degree of orientation (002) plane and a degree of orientation relation, $F(hkl)$, is given below [33]:

$$F(hkl) = \frac{P(hkl) - P_o(hkl)}{1 - P_o(hkl)} \quad (1)$$

where, $P(hkl) = I(hkl)/\sum I(hkl)$ and $P_o(hkl) = I_o(hkl)/\sum I_o(hkl)$. Here, $I(hkl)$ is the (hkl) peak intensity and $\sum I(hkl)$ is the sum of the intensities of all peaks. $I_o(hkl)$ is the (hkl) peak intensity and $\sum I_o(hkl)$ is the sum of the intensities of diffraction peaks in the reference data (JCPDS 36-1451) [34]. Fig. 1(b) shows the degree of orientation (002) and the peak intensity (002) versus annealing temperature. The maximum degree of orientation (002) was observed for the film annealed at 600 °C. It reveals that the preferred c-axis orientation along (002) plane was improved as the annealing temperature increased to 600 °C. Beyond the annealing temperature of 600 °C, the degree of (002) orientation decreased, it means that the other weak peaks corresponding to (101) and (100) planes were enhanced. The possible occurrence of the weak peak at the high annealing temperature, is related to the recrystallization of YZO thin films. At the high annealing temperature, the sufficient thermal energy was achieved to diffuse smaller crystals into larger ones. Compared to ZnO thin films, the crystalline phase of YZO films were gained enough energy to orient themselves along (002) plane annealed at 600 °C [33, 35]. On the other hand, the peak intensity (002) increased and the FWHM decreased due to the improvement of the crystallinity of YZO thin films as the annealing temperature increased from 300 °C to 600 °C. The crystallite size of YZO thin films was evaluated from the Scherrer's formula [36]:

$$D = \frac{0.94\lambda}{\beta \cos \theta}$$

where, λ is the X-ray wavelength (0.154 nm), θ is the Bragg diffraction angle, and β is the full width at half maximum (FWHM). The estimated average grain size of YZO thin films were varied from 7.97 to 19.80 nm as the annealing temperature increased from 300 °C to 700 °C. The average grain size of YZO thin films evaluated from XRD peak profile analysis are summarized in the Table 1. The post heat treatment influenced the grain size of YZO thin films, which was also confirmed by FE-SEM micrographs (Fig. 2). The increasing grain size of YZO thin films with increasing annealing temperature could be observed due to the coalescence of small grains by the grain boundary diffusion caused major grain growth [37]. In-addition, some of the dangling defects or zinc and/or oxygen defects are favorable in merging process to form bigger grains [38]. Therefore, the lattice constant 'c', gradually decreased from 5.22 Å to 5.18 Å by increasing the annealing temperature from 300°C to 700°C due to the shifting of (002)

peak towards higher diffraction angle (Table 1). For YZO thin films annealed at 300 - 500 °C, the ‘c’, was observed to be larger than that of the bulk ZnO (5.20 Å) [39], which indicates the elongation of unit cell along c-axis and the compressive forces act in the plane of the film [40]. Beyond the annealing temperature ≥ 600 °C, ‘c’ reduced to 5.18 Å. The decreasing of the ‘c’ of YZO thin film might be attributed to the lattice contraction and the presence of dangling bonds consist of Zn^{2+} and O^{2-} ions on the surface of thin films [41, 42]. The variation in lattice parameter, ‘c’, clearly indicates the relaxation of the residual stress by annealing at high temperature.

In order to understand the transition of residual stress of YZO thin film by post annealing, the linear stress-strain relations of hexagonal ZnO crystals can be described as [26]:

$$\begin{bmatrix} \sigma_{11} \\ \sigma_{22} \\ \sigma_{33} \end{bmatrix} = \begin{bmatrix} C_{11} & C_{12} & C_{13} \\ C_{21} & C_{22} & C_{23} \\ C_{31} & C_{32} & C_{33} \end{bmatrix} \begin{bmatrix} \epsilon_{11} \\ \epsilon_{22} \\ \epsilon_{33} \end{bmatrix} \quad (2)$$

Where C_{ij} are elastic constants; σ_{ij} and ϵ_{ij} are normal stresses and strains, respectively. By assuming only the biaxial stresses occur in thin films, i.e., $\sigma_{33}=0$ (free surface condition)

$$\epsilon_{11} + \epsilon_{22} = -\epsilon_{33} \frac{C_{33}}{C_{13}} \quad (3)$$

If in-plane stress is isotropic, ($\sigma_{11}=\sigma_{22}$), then the equation can be described as:

$$\sigma_{11} = \frac{2C_{13}^2 - C_{33}(C_{11} + C_{12})}{2C_{13}} * \epsilon_{33} \quad (4)$$

The strain along z-axis can be described in terms of c-axis lattice constants of film c_{film} and stress free bulk material c_{bulk}

$$\varepsilon_{33} = \frac{c_{\text{film}} - c_{\text{bulk}}}{c_{\text{bulk}}} \quad (5)$$

Then aforementioned equation (4) can be written as

$$\sigma = \frac{2C_{13}^2 - C_{33}(C_{11} + C_{12})}{2C_{13}} * \frac{c_{\text{film}} - c_{\text{bulk}}}{c_{\text{bulk}}} \quad (6)$$

The value of elastic constants are $C_{11} = 208.8$ GPa, $C_{12} = 119.7$ GPa, $C_{13} = 104.2$ GPa, $C_{33} = 213.8$ GPa, and c_{bulk} is the lattice constant of bulk ZnO (5.2071 Å). The variation of the residual stress with respect to the annealing temperature is shown in Table 1. The residual stress of as-deposited YZO thin films was observed to be -1.252 GPa, which was increased from -0.805 to 0.537 GPa as the annealing temperature increased from 400 °C to 700 °C. It can be seen that the nature of YZO thin films was initially compressive, which relaxed to tensile with an increase of the annealing temperature. This relaxation of residual stress could be expected due to the transfer of energy from annealing to the lattice of YZO. However, the other factors are also discussed for the purpose to complete understanding of relaxation of the residual stress phenomena in YZO thin films. Generally, the residual stress is contributed by the macroscopically stress (extrinsic stress) and microscopically stress (intrinsic stress).

However, in our case, it is anticipated that the total measured residual stress was caused by microscopically stress (intrinsic stress) such as intrinsic defects, impurities and lattice

distortion in the crystal structure. As it can be seen from the Table 1, the residual stress of as-deposited YZO thin films showed a compressive nature, which could be expected due to the structural defects freezing. These defects may include some dislocations, broken bonds which exist at the grain boundaries. As YZO thin films were started to anneal at 400 °C and 500 °C, the adsorbing atoms of films took very small energy to arrange themselves in the lowest energy state and developed more compressive (intrinsic) stress. When the annealing temperature reached to 600 °C, the relaxation of the residual stress was observed from a compressive to the tensile residual stress. It might be expected due to the high kinetic energy of thin films which results to increase the atomic mobility and reduce the defects. At the same time, some of the atoms in the films were started to migrate for obtaining enough energy at higher annealing temperature (600 °C and 700 °C) and the grains grew larger correspondingly, which agreed well with FE-SEM results [43].

Figs. 2 (a) - (e) show the surface images (FE-SEM) of as-deposited and annealed at 400°C, 500°C, 600°C, and 700°C of YZO (Y: 2 at.%) thin films, respectively. The grains were noticed on the film surfaces which grow preferentially along the c-axis perpendicular to the substrate. As the annealing temperature increased, the grains gradually started to grow up and at high annealing temperature, the atoms had enough diffusion activation energy to occupy the energetically favorite site in the crystal lattice. Lastly, the grains with lower surface energy became larger, which indicates the improved crystallinity of YZO thin films at high annealing temperature that consistent with the results of XRD pattern. The grain size obtained from the FE-SEM images was increased from ~6 nm to ~50 nm as the annealing temperature increased from 300 °C to 700 °C, respectively. The variation of grain size versus annealing temperature is shown in Fig. 2(f). **The grain boundary density with respect to the annealing temperature**

decreased due to the coarsening of inter-grain connections. However, the crystallite size calculated from XRD peak profile analysis was observed to be lower than that of the grain size noticed from FE-SEM analysis. It was expected that the grain size obtained from FE-SEM were usually composed of several crystallites [12, 44]. However, the earlier report of YZO thin films showed the voids, and Y content decreased by annealing [45]. Nevertheless, our results showed the fewer voids and good crystal quality of YZO thin films synthesized by the least expensive way and vacuum annealed.

Fig. 3 (a) shows the transmittance spectra of as-deposited and annealed of YZO (2 at.%) thin films. The absorbance spectra of YZO films is an inset of Fig. 3(a). The transmittance of YZO films under visible range slightly increased to 95% with respect to the annealing temperature of 400°C, 500°C and 600 °C and then decreased to 75% as the annealing temperature increased to 700 °C. The higher transmittance of YZO films indicates that the crystallinity was obtained better by annealing [46]. However, the absorption edge shifted towards higher wavelength region with the increasing of annealing temperature. The optical bandgap of YZO thin films were calculated from the fundamental absorption, which corresponding to electron excitation from valence band to the conduction band. The relation between the absorption coefficient (α) and incident photon energy ($h\nu$) is given by the equation [48]:

$$(\alpha \cdot h\nu)^{1/\gamma} = A(h\nu - E_g) \quad (7)$$

where, A is the proportionality constant, E_g is the bandgap of the material, γ depends upon the type of transition, $\gamma = 1/2, 2, 3/2$ and 3 corresponding to allowed direct, indirect, and/or forbidden band, respectively. With the value of $\gamma = 1/2$, direct optical bandgap were calculated from $(\alpha h\nu)^{1/\gamma}$

vs hv plot by extrapolating the linear portion of the graph to hv axis as shown in Fig 3 (b). The direct bandgap of YZO thin films were evaluated by taking the intercept on the hv axis (x-axis). The bandgap decreased from 3.28 eV to 3.22 eV as the annealing temperatures increased from 300 °C to 600 °C and then, it increased to 3.26 eV as the annealing temperatures increased to 700°C. Various factors can be contributed in the variation of optical bandgap with increasing of the annealing temperature. It might be occurred due to the thermal expansion which varied the periodic potential of electrons with temperature. Also, the effect of lattice vibrations changed the band structure and the bandgap of thin films with increasing the annealing temperature. These two factors are equivalent important to decrease the optical bandgap [47]. Moreover, it was previously reported that the stress or strain change the interatomic spacing of the semiconductors, which could affect the bandgap energy [48]. The energy gap increased as the tensile stress increased along the c-axis while decreased as the compressive stress increased [49]. Therefore, the bandgap of YZO thin films decreased with the increasing of annealing temperature and it could be expected due to the increase of compressive stresses. The other contributing factor to the reduction in bandgap may arise from the increase of the grain size with increasing the annealing temperature. When the grain size is small, the quantum confinement effect becomes significant, thus the bandgap showed a red shift with increased the grain size, as described by the following equation:

$$E_{g,nanocrystal} = E_{g,bulk} + \frac{\pi^2 \hbar^2}{2R^2} \left(\frac{1}{m_e^*} + \frac{1}{m_h^*} \right) \quad (8)$$

where, $E_{g,\text{nanocrystal}}$ and $E_{g,\text{bulk}}$ are the bandgaps of nanocrystalline films and the bulk materials, respectively. Therefore, the variation in bandgap can be attributed due to the increase in the grain size and stress relieving process of YZO thin films.

Furthermore, the absorption band edge of as-deposited and annealed YZO thin films can be determined from the position of the maximum of first derivative (dT/dE) of the optical transmittance [50], as shown in Fig. 4. The values of optical bandgap of YZO thin films are given in Table 2. The results indicate that the variation of bandgap of YZO (2 at.%) thin films was attained with respect to the annealing temperature. To summarize the bandgap of YZO thin films (Table 2) evaluated from two methods, it has worth noting that the bandgap was agreed well.

To estimate the other optical constants, such as, refractive index, n , extinction coefficient, k , and dielectric parameters, ϵ , the Swanepoel's method [50, 51] was used for the evaluation of optical constants of as-deposited and annealed YZO thin films by creating upper and lower envelopes of the transmission spectra. The following equations are used for the calculation of the refractive index:

$$n = \sqrt{N + \sqrt{N^2 - S^2}} \quad (9)$$

$$N = 2S \frac{T_M - T_m}{T_M T_m} + \frac{S^2 + 1}{2} \quad (10)$$

Here, S is the refractive index of the glass substrate (1.45), T_M and T_m are the values of transmission maximum and minimum at the wavelengths of the upper and lower envelopes,

respectively. It can be seen from Figs. 5 (a) and (b) that there was no considerable changes observed in the visible region of YZO thin films. However, the refractive index of YZO thin films in the UV region were observed larger than the visible region and increased with an increasing of the annealing temperature. We are reporting first time for the variation of refractive index of YZO thin films, which is an important parameter for the application of optoelectronic devices. However, the refractive index of ZnO thin films increased with increasing the annealing temperature up to 673 K [40]. In our case, the refractive index of YZO (2 at.%) thin films increased with the increasing of annealing temperature up to 600 °C due to decreasing of the bandgap. Therefore, it might be concluded that the smaller bandgap energy materials have higher refractive index [52]. However, the bandgap of YZO thin film increased at the high annealing temperature increased to 700 °C. Further increase in the refractive index at high temperature annealing (700 °C) of YZO thin films might be assigned due to the increasing grain size. So, post deposition annealing of YZO thin films was found to increase the refractive index significantly due to the contribution of the bandgap and grain size. The extinction coefficient calculated from the absorption coefficient (α) by using the formula:

$$k = \frac{\alpha\lambda}{4\pi} \quad (11)$$

The extinction coefficient was observed to be varied a little in the visible region, which indicated that all deposited films were almost transparent in the visible region and consistent with the results of transmission spectra. The extinction coefficient was observed to be higher for YZO films annealed at the highest annealing temperature of 700°C than the YZO films annealed at the lower annealing temperature of 400 - 600°C due to lower transmittance in the visible region.

The complex dielectric constant of all YZO thin films was calculated by using the relation as given below:

$$\varepsilon(\lambda) = \varepsilon_r(\lambda) - i\varepsilon_i(\lambda) \quad (12)$$

where, real (ε_r) and imaginary (ε_i) components of dielectric constants and they are related to n and k values. The ε_r and ε_i values were calculated from using following formulas:

$$\varepsilon_r(\lambda) = n^2(\lambda) - k^2(\lambda) \quad (13)$$

$$\varepsilon_i(\lambda) = 2n(\lambda)k(\lambda) \quad (14)$$

The variation of real (ε_r) and imaginary (ε_i) components of the dielectric constant of annealed YZO (2 at.%) thin films are shown in Fig. 6. The real and imaginary dielectric constants were increased by increasing the annealing temperatures of YZO (2 at.%) thin films. It is reported that the real and imaginary component of the dielectric constant provide the information about electronic band structure [53]. Moreover, the real dielectric constant is observed higher than that of the imaginary dielectric constant, which indicates the good transparency of YZO thin films. From the optical data, it was noticed that the n , k , ε_r and ε_i followed the same behavior as a function of the wavelength in all annealed YZO thin films. Therefore, the optical properties of YZO thin films can be controlled by the appropriate dopant (Y) concentration and post annealing at a specified temperature that might be important in view of designing the optical devices.

Fig. 7(a) shows the PL spectra of as-deposited and annealed (400 - 700 °C) YZO thin films. The PL spectra of as-deposited YZO thin film is composed of two peaks. The first peak at 368 nm (3.36 eV) was usually referred to the intensity of UV emission while other broad band peak centered in the vicinity of 542 nm (2.28 eV) was observed, named as green-yellow emission. As the post-annealing temperature increased from 400 °C to 600 °C, the UV peak or the near band edge peak (NBE) associated with band-to-band recombination was red shifted from 386 nm to 397 nm, coinciding roughly with the bandgap derived from transmission spectra. The shifting of bandgap energy was related to stress phenomena which caused to structural changes. As the compressed stress increased and then relaxed to the tensile stress, correspondingly the bandgap energy related to UV peak was decreased. Further increasing of the annealing temperature from 600 °C to 700 °C, the UV peak was blue shifted to 372 nm and correspondingly the bandgap increased which was also noticed in the bandgap obtained by fitting the $(ahv)^2$ vs hv plot. Therefore, the shifting of UV peak towards higher or lower wavelength side could be related to the nature of the variation of bandgap. Moreover, the intensity of UV peak was increased for YZO thin films annealed up to 600 °C and then decreased for the film annealed at 700°C. Generally, the correlation between the intensity of UV or NBE peak with the crystallinity of thin films has been reported [54-56]. **The peak (002) intensity of YZO thin films increased as the annealing temperature increased to 700 °C. Beyond the annealing temperature \geq 600 °C, the other peaks (100) and (101) intensity of YZO thin films were also increased as the annealing temperature increased to 700°C. Thus, the degree of orientation of (002) peak (Fig. 1b) started to decrease with increasing of (100) and (101) orientation peaks of YZO thin films annealed at 700 °C. The orientation of other peaks are related to the oxygen defects which might be attributed to the transition between the excited electrons**

and oxygen related defect centers, which leads to the visible emission. From increasing the defect centers at the highest annealing temperature of 700 °C, the recombination efficiency of free excitons become lower to emit UV light. Therefore, the UV peak intensity of YZO thin film was decreased as the annealing temperature extended to 700 °C.

After analyzing the annealing effect on UV peaks of YZO thin films, the visible emission was systematically analyzed to investigate the origin of deep level defects. The visible emission of PL peak of as-deposited YZO thin films was located at 542 nm (2.28 eV) which extremely showing the broad green-yellow emission band. The origin of green-yellow emission is related to the structural defects [57-59]. The nonstoichiometric defects, such as, zinc vacancy, antisite defects were also associated to cause the deep level emission of ZnO thin films during film growth [60, 61]. Therefore, a number of lattice and structural defects are expected in as-deposited and low temperature annealing of YZO thin films. As the annealing temperature increased to 400 °C the broad emission band was shifted towards higher wavelength region 576 nm (2.15 eV) with a little suppression of intensity. At the annealing temperature of 500 °C, the UV peak was shifted from 3.32 to 3.20 eV. While the DLE peak was suppressed and moved towards higher energy band from 2.15 to 2.50 eV. The YZO films annealed at 500 °C, the yellow peak was completely diminished and green emission band was observed. Thus, it is believed that the emission of the green band region was expected to the recombination of conduction band electrons with holes, which trapped at oxygen vacancies. Also, the green emission is generally assigned to the transition between a singly charged oxygen vacancy and a photo-excited hole [62]. In addition, the recently theoretical report by Janotti and Van de walle [63] and experimentally by Reynolds et Al. [64] demonstrated that the transitions from the conduction band or a shallow donor level to singly ionized Zn vacancies, which was possible with the

corresponding energy of 2.5 eV. Moreover, the green emission (2.5 eV) of ZnO thin films were reported due to oxygen interstitials or zinc vacancies grown in oxygen rich environment [65]. In our case, the green emission (2.5 eV) of YZO thin films were also observed for the films annealed at 500 °C in vacuum due to the singly oxygen vacancies rather than zinc vacancies [66]. This green emission band was completely diminished when the annealing temperature of YZO thin film reached to 600 °C. One broad peak was observed in the range 350-500 nm and fitted by deconvolution of two Gaussians curves (Fig 7 b), which showed the existence of two kind of peaks centered at 3.1 eV (UV emission) and 2.7 eV (blue emission). The blue emission of YZO thin films annealed at 600 °C could be expected due to electronic transitions from the conduction band to the acceptor level (antisite oxygen defects). Likewise, Ding et al. [67] reported the origin of blue emission (2.7 eV) in the AZO thin films annealed in vacuum. Wei et al. [68] also demonstrated the blue emission peak at 459 nm (2.6 eV) for ZnO thin films annealed in vacuum, O₂ and N₂ atmospheres. As a result, the blue emission of YZO thin films might be expected due to the vacuum annealing which leads to the transition between the conduction band to the acceptor level. While at the highest annealing temperature of 700 °C, the blue emission band of YZO thin films was completely diminished and observed an orange-red emission band at a wavelength of 610 nm (2.03 eV). Many reports have been proposed to understand the origination of orange-red emission band and it is still unclear. In the case of YZO thin films annealed at 700 °C, the orange-red emission might be attributed due to the other peak orientations of (100) and (101) that are related to oxygen defects. Ianno et al. [69] also reported the similar behavior in ZnO thin films. Some of the previous research reports also reported that the interstitial oxygen defects and Zn_i defects were responsible for the red-orange emission [66, 70-72]. Therefore, the

initiation of orange-red emission of YZO thin films annealed at 700 °C could be expected due to zinc interstitial atoms [55, 73], and oxygen related defects [58, 74].

4. CONCLUSION

In summary, YZO (2 at.%) thin films were prepared on the quartz glass substrates at room temperature by spin coating and subsequent annealed at 400~700 °C in vacuum. The vacuum annealing improved the crystallinity of YZO thin films. The grain size of YZO films were found to be increased by annealing. As the annealing temperature increased, the compressive stress tend to be relaxed and changed to tensile stress. Correspondingly, the changes in the bandgap energy might be predicted due to the variations in residual stress parameters. The optical constants, such as, refractive index (n), extinction coefficient (k), dielectric constants: real (ε_r) and imaginary (ε_i) increased with the increasing of annealing temperatures of YZO thin films, which can be attributed to the bandgap energy and structural modifications. The UV peak of annealed YZO thin films was also related to the bandgap transition which caused by the residual stress behavior. Therefore, it is found that the stress relaxation phenomena corresponding to the bandgap energy of YZO thin films was influenced by vacuum annealing at various temperatures.

Acknowledgements

This research was supported by the Basic Science Research Program (NRF-2013R1A1A2059900), funded by the Korean government of Ministry of Education (MoE).

REFERENCES

- [1] D. Lehr, M. Luka, M.R. Wagner, M. Bügler, A. Hoffmann, S. Polarz, Band-Gap Engineering of Zinc Oxide Colloids via Lattice Substitution with Sulfur Leading to Materials with Advanced Properties for Optical Applications Like Full Inorganic UV Protection, *Chemistry of Materials*, 24 (2012) 1771-1778.
- [2] C. Klingshirn, Review Article: ZnO: From basics towards applications, *physica status solidi (b)*, 244 (2007) 3019-3019.
- [3] S. Guo, Q. Hou, C. Zhao, Y. Zhang, Study of the effect of Cu heavy doping on band gap and absorption spectrum of ZnO, *Chemical Physics Letters*, 614 (2014) 15-20.
- [4] P.J. Rostan, U. Rau, V.X. Nguyen, T. Kirchartz, M.B. Schubert, J.H. Werner, Low-temperature a-Si:H/ZnO/Al back contacts for high-efficiency silicon solar cells, *Solar Energy Materials and Solar Cells*, 90 (2006) 1345-1352.
- [5] H.S. Al-Salman, M.J. Abdullah, RF sputtering enhanced the morphology and photoluminescence of multi-oriented ZnO nanostructure produced by chemical vapor deposition, *Journal of Alloys and Compounds*, 547 (2013) 132-137.
- [6] M. Shirazi, M.T. Hosseinnejad, A. Zendehnam, M. Ghoranneviss, G. Reza Etaati, Synthesis and characterization of nanostructured ZnO multilayer grown by DC magnetron sputtering, *Journal of Alloys and Compounds*, 602 (2014) 108-116.
- [7] J.-H. Lee, B.-O. Park, Characteristics of Al-doped ZnO thin films obtained by ultrasonic spray pyrolysis: effects of Al doping and an annealing treatment, *Materials Science and Engineering: B*, 106 (2004) 242-245.
- [8] F.K. Shan, G.X. Liu, W.J. Lee, G.H. Lee, I.S. Kim, B.C. Shin, Y.C. Kim, Transparent conductive ZnO thin films on glass substrates deposited by pulsed laser deposition, *Journal of Crystal Growth*, 277 (2005) 284-292.

- [9] M. Lange, C.P. Dietrich, K. Brachwitz, T. Böntgen, M. Lorenz, M. Grundmann, (Zn,Cd)O thin films for the application in heterostructures: Structural and optical properties, *Journal of Applied Physics*, 112 (2012) 103517.
- [10] Z. Fu, B. Lin, J. Zu, Photoluminescence and structure of ZnO films deposited on Si substrates by metal-organic chemical vapor deposition, *Thin Solid Films*, 402 (2002) 302-306.
- [11] P. Jongnavakit, P. Amornpitoksuk, S. Suwanboon, T. Ratana, Surface and photocatalytic properties of ZnO thin film prepared by sol-gel method, *Thin Solid Films*, 520 (2012) 5561-5567.
- [12] G. Li, X. Zhu, X. Tang, W. Song, Z. Yang, J. Dai, Y. Sun, X. Pan, S. Dai, Doping and annealing effects on ZnO:Cd thin films by sol-gel method, *Journal of Alloys and Compounds*, 509 (2011) 4816-4823.
- [13] M.H. Tang, Z.Q. Zeng, J.C. Li, Z.P. Wang, X.L. Xu, G.Y. Wang, L.B. Zhang, S.B. Yang, Y.G. Xiao, B. Jiang, Resistive switching behavior of La-doped ZnO films for nonvolatile memory applications, *Solid-State Electronics*, 63 (2011) 100-104.
- [14] R. Zamiri, A.F. Lemos, A. Reblo, H.A. Ahangar, J.M.F. Ferreira, Effects of rare-earth (Er, La and Yb) doping on morphology and structure properties of ZnO nanostructures prepared by wet chemical method, *Ceramics International*, 40 (2014) 523-529.
- [15] Y.-Z. Tsai, N.-F. Wang, M.-R. Tseng, F.-H. Hsu, Transparent conducting Al and Y codoped ZnO thin film deposited by DC sputtering, *Materials Chemistry and Physics*, 123 (2010) 300-303.
- [16] T. Minami, T. Yamamoto, T. Miyata, Highly transparent and conductive rare earth-doped ZnO thin films prepared by magnetron sputtering, *Thin Solid Films*, 366 (2000) 63-68.
- [17] S. Heo, S.K. Sharma, S. Lee, Y. Lee, C. Kim, B. Lee, H. Lee, D.Y. Kim, Effects of Y contents on surface, structural, optical, and electrical properties for Y-doped ZnO thin films, *Thin Solid Films*, 558 (2014) 27-30.

- [18] S.K. Sharma, D.V.N. Sudheer Pamidimarri, D.Y. Kim, J.-G. Na, Y-doped zinc oxide (YZO) nanoflowers, microstructural analysis and test their antibacterial activity, Materials Science and Engineering: C, 53 (2015) 104-110.
- [19] W. Guo, T. Liu, R. Sun, Y. Chen, W. Zeng, Z. Wang, Hollow, porous, and yttrium functionalized ZnO nanospheres with enhanced gas-sensing performances, Sensors and Actuators B: Chemical, 178 (2013) 53-62.
- [20] A. Mahmood, A. Nadeem, Q. Raza, K. Taj Muhammad, M. Mehmood, M.M. Hassan, N. Mahmood, Effect of thermal annealing on the structural and optical properties of ZnO thin films deposited by the reactive e-beam evaporation technique, Physica Scripta, 82 (2010) 065801.
- [21] Y. Qingjiang, F. Wuyou, Y. Cuiling, Y. Haibin, W. Ronghui, S. Yongming, L. Shikai, L. Zhanlian, L. Minghui, W. Guorui, S. Changlu, L. Yichun, Z. Guangtian, Structural, electrical and optical properties of yttrium-doped ZnO thin films prepared by sol-gel method, Journal of Physics D: Applied Physics, 40 (2007) 5592.
- [22] M.-C. Jun, S.-U. Park, J.-H. Koh, Comparative studies of Al-doped ZnO and Ga-doped ZnO transparent conducting oxide thin films, Nanoscale Res Lett, 7 (2012) 639.
- [23] S. Heo, Y. Lee, S.K. Sharma, S. Lee, D.Y. Kim, Mole-controlled growth of Y-doped ZnO nanostructures by hydrothermal method, Current Applied Physics, 14 (2014) 1576-1581.
- [24] M.F. Malek, M.H. Mamat, M.Z. Sahdan, M.M. Zahidi, Z. Khusaimi, M.R. Mahmood, Influence of various sol concentrations on stress/strain and properties of ZnO thin films synthesised by sol-gel technique, Thin Solid Films, 527 (2013) 102-109.
- [25] Y.F. Li, B. Yao, Y.M. Lu, Y.Q. Gai, C.X. Cong, Z.Z. Zhang, D.X. Zhao, J.Y. Zhang, B.H. Li, D.Z. Shen, X.W. Fan, Z.K. Tang, Biaxial stress-dependent optical band gap, crystalline, and electronic structure in wurtzite ZnO: Experimental and ab initio study, Journal of Applied Physics, 104 (2008) 083516.

- [26] C.-H. Li, J.-Z. Chen, I.-C. Cheng, Transitions of bandgap and built-in stress for sputtered HfZnO thin films after thermal treatments, *Journal of Applied Physics*, 114 (2013) 084503.
- [27] T.P. Rao, M.C.S. Kumar, S.A. Angayarkanni, M. Ashok, Effect of stress on optical band gap of ZnO thin films with substrate temperature by spray pyrolysis, *Journal of Alloys and Compounds*, 485 (2009) 413-417.
- [28] Y. Hwang, S. Park, M. Kang, Y. Um, Effects of temperature-induced stress on the structural, electrical, and optical properties of ZnO:Ga thin films grown on Si substrates, *Current Applied Physics*, 14, Supplement 1 (2014) S23-S28.
- [29] R. Kumar, N. Khare, V. Kumar, G.L. Bhalla, Effect of intrinsic stress on the optical properties of nanostructured ZnO thin films grown by rf magnetron sputtering, *Applied Surface Science*, 254 (2008) 6509-6513.
- [30] C.-H. Li, J.-Z. Chen, Electrical, optical, and microstructural properties of sol-gel derived HfZnO thin films, *Journal of Alloys and Compounds*, 601 (2014) 223-230.
- [31] Q. Guoqiang, Z. Guanglei, L. Dongchun, L. Shimin, Lattice and internal relaxation of ZnO thin film under in-plane strain, *Thin Solid Films*, 519 (2010) 378-384.
- [32] T. Singh, T. Lehnert, T. Leuning, D. Sahu, S. Mathur, Thickness dependence of optoelectronic properties in ALD grown ZnO thin films, *Applied Surface Science*, 289 (2014) 27-32.
- [33] J. Sengupta, R.K. Sahoo, K.K. Bardhan, C.D. Mukherjee, Influence of annealing temperature on the structural, topographical and optical properties of sol-gel derived ZnO thin films, *Materials Letters*, 65 (2011) 2572-2574.
- [34] X.L. Zhang, K.S. Hui, F. Bin, K.N. Hui, L. Li, Y.R. Cho, R.S. Mane, W. Zhou, Effect of thermal annealing on the structural, electrical and optical properties of Al-Ni co-doped ZnO thin films prepared using a sol-gel method, *Surface and Coatings Technology*, 261 (2015) 149-155.

- [35] Z. Jiwei, Z. Liangying, Y. Xi, The dielectric properties and optical propagation loss of c-axis oriented ZnO thin films deposited by sol–gel process, Ceramics International, 26 (2000) 883-885.
- [36] C. Liu, Z. Xu, Y. Zhang, J. Fu, S. Zang, Y. Zuo, Effect of annealing temperature on properties of ZnO:Al thin films prepared by pulsed DC reactive magnetron sputtering, Materials Letters, 139 (2015) 279-283.
- [37] Y. Caglar, S. Ilican, M. Caglar, F. Yakuphanoglu, J. Wu, K. Gao, P. Lu, D. Xue, Influence of heat treatment on the nanocrystalline structure of ZnO film deposited on p-Si, Journal of Alloys and Compounds, 481 (2009) 885-889.
- [38] Y. Lin, J. Xie, H. Wang, Y. Li, C. Chavez, S. Lee, S.R. Foltyn, S.A. Crooker, A.K. Burrell, T.M. McCleskey, Q.X. Jia, Green luminescent zinc oxide films prepared by polymer-assisted deposition with rapid thermal process, Thin Solid Films, 492 (2005) 101-104.
- [39] R.D. Vispute, V. Talyansky, S. Choopun, R.P. Sharma, T. Venkatesan, M. He, X. Tang, J.B. Halpern, M.G. Spencer, Y.X. Li, L.G. Salamanca-Riba, A.A. Iliadis, K.A. Jones, Heteroepitaxy of ZnO on GaN and its implications for fabrication of hybrid optoelectronic devices, Applied Physics Letters, 73 (1998) 348-350.
- [40] V. Gupta, A. Mansingh, Influence of postdeposition annealing on the structural and optical properties of sputtered zinc oxide film, Journal of Applied Physics, 80 (1996) 1063-1073.
- [41] O. Lupon, T. Pauporté, L. Chow, B. Viana, F. Pellé, L.K. Ono, B. Roldan Cuenya, H. Heinrich, Effects of annealing on properties of ZnO thin films prepared by electrochemical deposition in chloride medium, Applied Surface Science, 256 (2010) 1895-1907.
- [42] M.F. Malek, M.H. Mamat, Z. Khusaimi, M.Z. Sahdan, M.Z. Musa, A.R. Zainun, A.B. Suriani, N.D. Md Sin, S.B. Abd Hamid, M. Rusop, Sonicated sol–gel preparation of nanoparticulate ZnO thin films with various deposition speeds: The highly preferred c-axis (0°; 90°) orientation enhances the final properties, Journal of Alloys and Compounds, 582 (2014) 12-21.

- [43] P.R. Berger, K. Chang, P. Bhattacharya, J. Singh, K.K. Bajaj, Role of strain and growth conditions on the growth front profile of $In_xGa_{1-x}As$ on GaAs during the pseudomorphic growth regime, *Applied Physics Letters*, 53 (1988) 684-686.
- [44] L. Xu, F. Gu, J. Su, Y. Chen, X. Li, X. Wang, The evolution behavior of structures and photoluminescence of K-doped ZnO thin films under different annealing temperatures, *Journal of Alloys and Compounds*, 509 (2011) 2942-2947.
- [45] P.-T. Hsieh, R.W.-K. Chuang, C.-Q. Chang, C.-M. Wang, S.-J. Chang, Optical and structural characteristics of yttrium doped ZnO films using sol-gel technology, *Journal of sol-gel science and technology*, 58 (2011) 42-47.
- [46] M. Rusop, K. Uma, T. Soga, T. Jimbo, Post-growth annealing of zinc oxide thin films pulsed laser deposited under enhanced oxygen pressure on quartz and silicon substrates, *Materials Science and Engineering: B*, 127 (2006) 150-153.
- [47] G.P. Daniel, V.B. Justinvictor, P.B. Nair, K. Joy, P. Koshy, P.V. Thomas, Effect of annealing temperature on the structural and optical properties of ZnO thin films prepared by RF magnetron sputtering, *Physica B: Condensed Matter*, 405 (2010) 1782-1786.
- [48] M.F. Malek, M.H. Mamat, M.Z. Musa, Z. Khusaimi, M.Z. Sahdan, A.B. Suriani, A. Ishak, I. Saurdi, S.A. Rahman, M. Rusop, Thermal annealing-induced formation of ZnO nanoparticles: Minimum strain and stress ameliorate preferred c-axis orientation and crystal-growth properties, *Journal of Alloys and Compounds*, 610 (2014) 575-588.
- [49] R. Ghosh, D. Basak, S. Fujihara, Effect of substrate-induced strain on the structural, electrical, and optical properties of polycrystalline ZnO thin films, *Journal of Applied Physics*, 96 (2004) 2689-2692.
- [50] F.Z. Bedia, A. Bedia, N. Maloufi, M. Aillerie, F. Genty, B. Benyoucef, Effect of tin doping on optical properties of nanostructured ZnO thin films grown by spray pyrolysis technique, *Journal of Alloys and Compounds*, 616 (2014) 312-318.

- [51] S.K. Sharma, J. Baveja, R.M. Mehra, The Dependence of Optical Constants on Selenium and Sulphur-Doping in a-Si:H, *physica status solidi (a)*, 194 (2002) 216-225.
- [52] M.A. Yıldırım, S.T. Yıldırım, E.F. Sakar, A. Ateş, Synthesis, characterization and dielectric properties of SnO₂ thin films, *Spectrochimica Acta Part A: Molecular and Biomolecular Spectroscopy*, 133 (2014) 60-65.
- [53] R. Mariappan, V. Ponnuswamy, P. Suresh, R. Suresh, M. Ragavendar, A. Chandra Bose, Nanostructured Ce_xZn_{1-x}O thin films: Influence of Ce doping on the structural, optical and electrical properties, *Journal of Alloys and Compounds*, 588 (2014) 170-176.
- [54] S. Im, B.J. Jin, S. Yi, Ultraviolet emission and microstructural evolution in pulsed-laser-deposited ZnO films, *Journal of Applied Physics*, 87 (2000) 4558-4561.
- [55] O. Kenichi, G. Manabu, Strong Ultraviolet Photoluminescence in Polycrystalline ZnO Sputtered Films, *Japanese Journal of Applied Physics*, 41 (2002) 5614.
- [56] F.K. Shan, B.I. Kim, G.X. Liu, Z.F. Liu, J.Y. Sohn, W.J. Lee, B.C. Shin, Y.S. Yu, Blueshift of near band edge emission in Mg doped ZnO thin films and aging, *Journal of Applied Physics*, 95 (2004) 4772-4776.
- [57] X.L. Wu, G.G. Siu, C.L. Fu, H.C. Ong, Photoluminescence and cathodoluminescence studies of stoichiometric and oxygen-deficient ZnO films, *Applied Physics Letters*, 78 (2001) 2285-2287.
- [58] K. Vanheusden, W.L. Warren, C.H. Seager, D.R. Tallant, J.A. Voigt, B.E. Gnade, Mechanisms behind green photoluminescence in ZnO phosphor powders, *Journal of Applied Physics*, 79 (1996) 7983-7990.
- [59] X. Jin, M. Götz, S. Wille, Y.K. Mishra, R. Adelung, C. Zollfrank, A Novel Concept for Self-Reporting Materials: Stress Sensitive Photoluminescence in ZnO Tetrapod Filled Elastomers, *Advanced Materials*, 25 (2013) 1342-1347.
- [60] R. Ayouchi, F. Martin, D. Leinen, J.R. Ramos-Barrado, Growth of pure ZnO thin films prepared by chemical spray pyrolysis on silicon, *Journal of Crystal Growth*, 247 (2003) 497-504.

- [61] S. Yamauchi, Y. Goto, T. Hariu, Photoluminescence studies of undoped and nitrogen-doped ZnO layers grown by plasma-assisted epitaxy, *Journal of Crystal Growth*, 260 (2004) 1-6.
- [62] K. Vanheusden, C.H. Seager, W.L. Warren, D.R. Tallant, J.A. Voigt, Correlation between photoluminescence and oxygen vacancies in ZnO phosphors, *Applied Physics Letters*, 68 (1996) 403-405.
- [63] A. Janotti, C.G. Van de Walle, Native point defects in ZnO, *Physical Review B*, 76 (2007) 165202.
- [64] D.C. Reynolds, D.C. Look, B. Jogai, H. Morkoç, Similarities in the bandedge and deep-centre photoluminescence mechanisms of ZnO and GaN, *Solid State Communications*, 101 (1997) 643-646.
- [65] M.N. Islam, T.B. Ghosh, K.L. Chopra, H.N. Acharya, XPS and X-ray diffraction studies of aluminum-doped zinc oxide transparent conducting films, *Thin Solid Films*, 280 (1996) 20-25.
- [66] C.H. Ahn, Y.Y. Kim, D.C. Kim, S.K. Mohanta, H.K. Cho, Erratum: "A comparative analysis of deep level emission in ZnO layers deposited by various methods" [J. Appl. Phys. 105, 013502 (2009)], *Journal of Applied Physics*, 105 (2009) 089902.
- [67] J.J. Ding, H.X. Chen, S.Y. Ma, The Al-doping and post-annealing treatment effects on the structural and optical properties of ZnO:Al thin films deposited on Si substrate, *Applied Surface Science*, 256 (2010) 4304-4309.
- [68] X.Q. Wei, B.Y. Man, M. Liu, C.S. Xue, H.Z. Zhuang, C. Yang, Blue luminescent centers and microstructural evaluation by XPS and Raman in ZnO thin films annealed in vacuum, N₂ and O₂, *Physica B: Condensed Matter*, 388 (2007) 145-152.
- [69] N.J. Ianno, L. McConville, N. Shaikh, S. Pittal, P.G. Snyder, Characterization of pulsed laser deposited zinc oxide, *Thin Solid Films*, 220 (1992) 92-99.
- [70] J.D. Ye, S.L. Gu, F. Qin, S.M. Zhu, S.M. Liu, X. Zhou, W. Liu, L.Q. Hu, R. Zhang, Y. Shi, Y.D. Zheng, Correlation between green luminescence and morphology evolution of ZnO films, *Applied Physics A*, 81 (2005) 759-762.

- [71] N.H. Alvi, K. ul Hasan, O. Nur, M. Willander, The origin of the red emission in n-ZnO nanotubes/p-GaN white light emitting diodes, *Nanoscale Research Letters*, 6 (2011) 130-130.
- [72] B. Yao, D.Z. Shen, Z.Z. Zhang, X.H. Wang, Z.P. Wei, B.H. Li, Y.M. Lv, X.W. Fan, L.X. Guan, G.Z. Xing, C.X. Cong, Y.P. Xie, Effects of nitrogen doping and illumination on lattice constants and conductivity behavior of zinc oxide grown by magnetron sputtering, *Journal of Applied Physics*, 99 (2006) 123510.
- [73] G. Manabu, O. Naoko, O. Kenichi, K. Mikio, Photoluminescent and Structural Properties of Precipitated ZnO Fine Particles, *Japanese Journal of Applied Physics*, 42 (2003) 481.
- [74] M. Liu, A.H. Kitai, P. Mascher, Point defects and luminescence centres in zinc oxide and zinc oxide doped with manganese, *Journal of Luminescence*, 54 (1992) 35-42.
- [75] S.-H. Jeong, B.-S. Kim, B.-T. Lee, Photoluminescence dependence of ZnO films grown on Si(100) by radio-frequency magnetron sputtering on the growth ambient, *Applied Physics Letters*, 82 (2003) 2625-2627.

Figures Caption:

Fig. 1 (a) XRD patterns of as-deposited and annealed YZO (2 at.%) thin films, (b) Variation of the orientation and intensity of XRD (002) peak with respect to the annealing temperature.

Fig. 2 (a ~ e) FE-SEM surface images of as-deposited and annealed (400 °C, 500 °C, 600 °C, and 700 °C) YZO (2 at.%) thin films, (f) variation of grain size calculated from FE-SEM images with respect to the annealing temperature.

Fig. 3 (a) Transmission and absorption spectra (inset) of as-deposited and annealed YZO (2 at.%) thin films, (b) $(\alpha h\nu)^2$ versus $h\nu$ plot of YZO (2 at.%) thin films with respect to the annealing temperature.

Fig. 4 dT/dE versus $h\nu$ plot of YZO (2 at.%) thin films annealed at 300 °C, 400 °C, 500 °C, 600 °C, and 700 °C in vacuum.

Fig. 5 Refractive index and extinction coefficient of YZO (2 at.%) thin films annealed at 300 °C, 400 °C, 500 °C, 600 °C, and 700 °C in vacuum.

Fig. 6 The real and imaginary (inset) component of dielectric constant of YZO (2 at.%) thin films annealed at 300 °C, 400 °C, 500 °C, 600 °C, and 700 °C in vacuum.

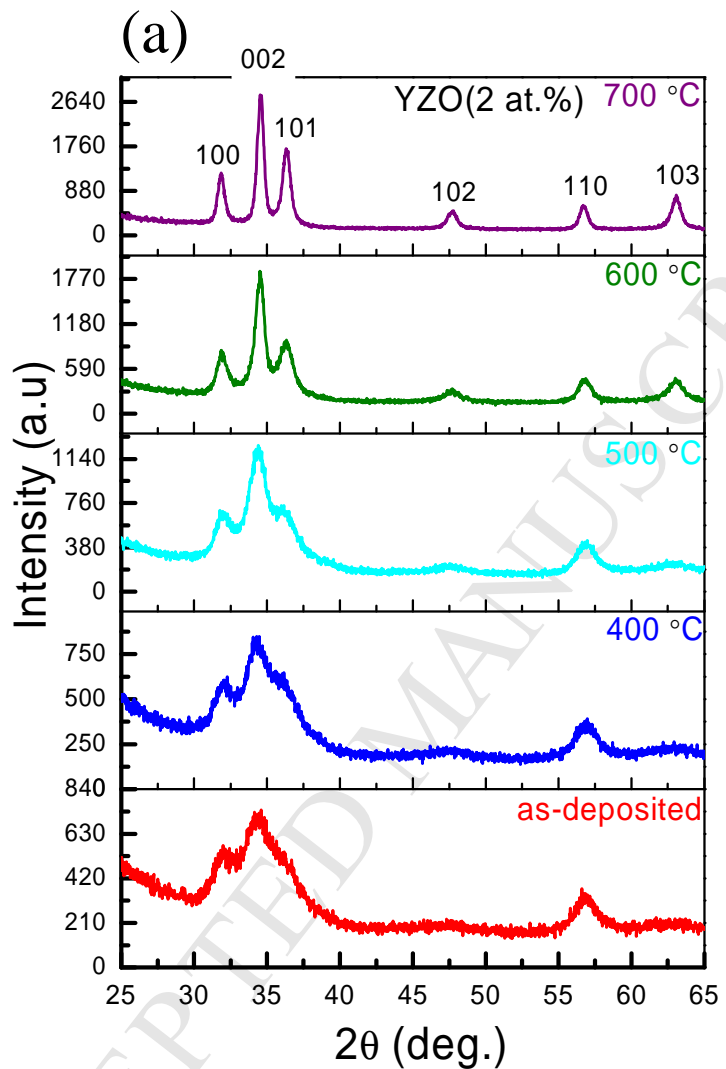
Fig. 7 (a) Room temperature PL spectra of as-deposited and annealed YZO (2 at.%) thin films, (b) Gaussian fits of PL spectra for visible emission of the YZO film annealed at the typical temperature of 600 °C.

Table 1 XRD parameters (FWHM, 2θ , crystal size, d-spacing, lattice constant, strain, residual stress) of as-deposited and annealed YZO thin films

Annealing Temperature (°C)	FWHM (β) (°)	Position (2θ) (002) plane	Crystal size (D) (nm)	d-spacing (Å)	Lattice constant (c) (Å)	Residual Stress (GPa)
300	1.09	34.27	7.97	2.614	5.228	-1.252
400	1.03	34.36	8.44	2.609	5.218	-0.805
500	0.91	34.39	9.52	2.605	5.210	-0.447
600	0.52	34.51	16.43	2.596	5.192	0.358
700	0.43	34.55	19.80	2.594	5.188	0.537

Table 2 Bandgap calculated from the Tauc's plot and dT/dE of YZO (2 at.%) thin films annealed at 300 °C, 400 °C, 500 °C, 600 °C and 700 °C in vacuum.

Annealing Temperature (°C)	Band gap (eV)	
	$(\alpha h\nu)^2$	dT/dE
300	3.28	3.28
400	3.25	3.22
500	3.23	3.21
600	3.22	3.19
700	3.26	3.27

Fig. 1

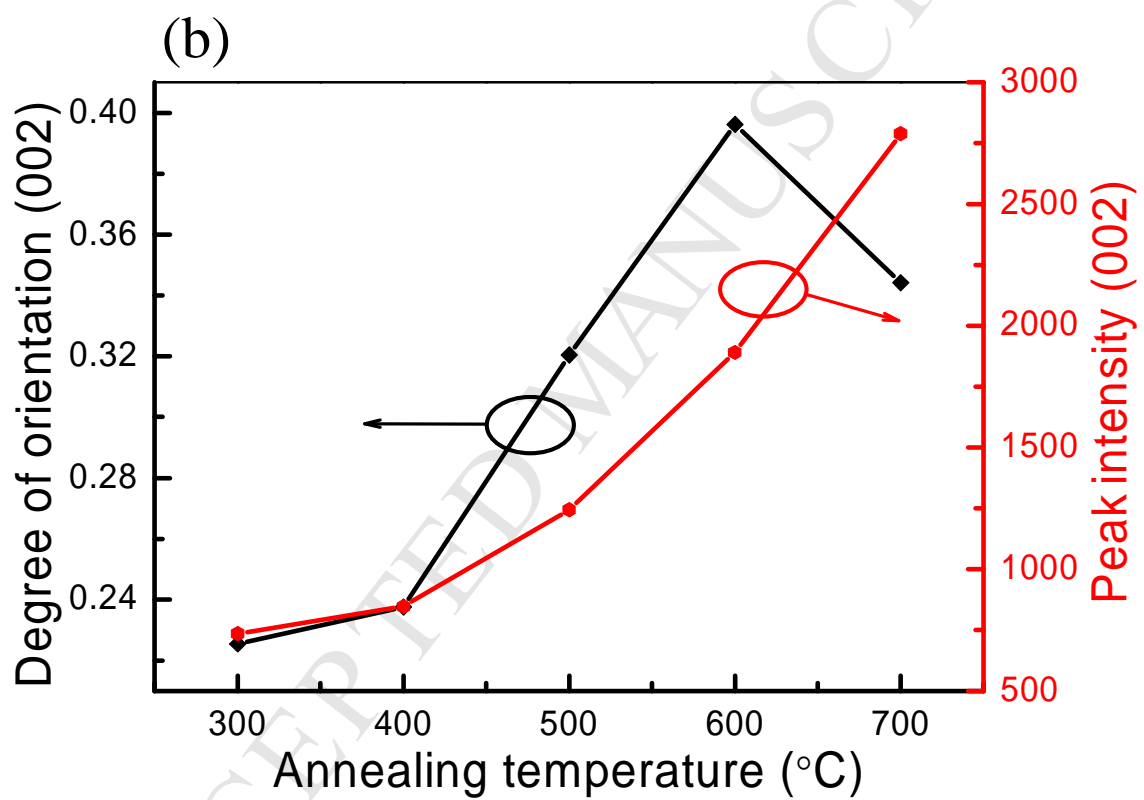


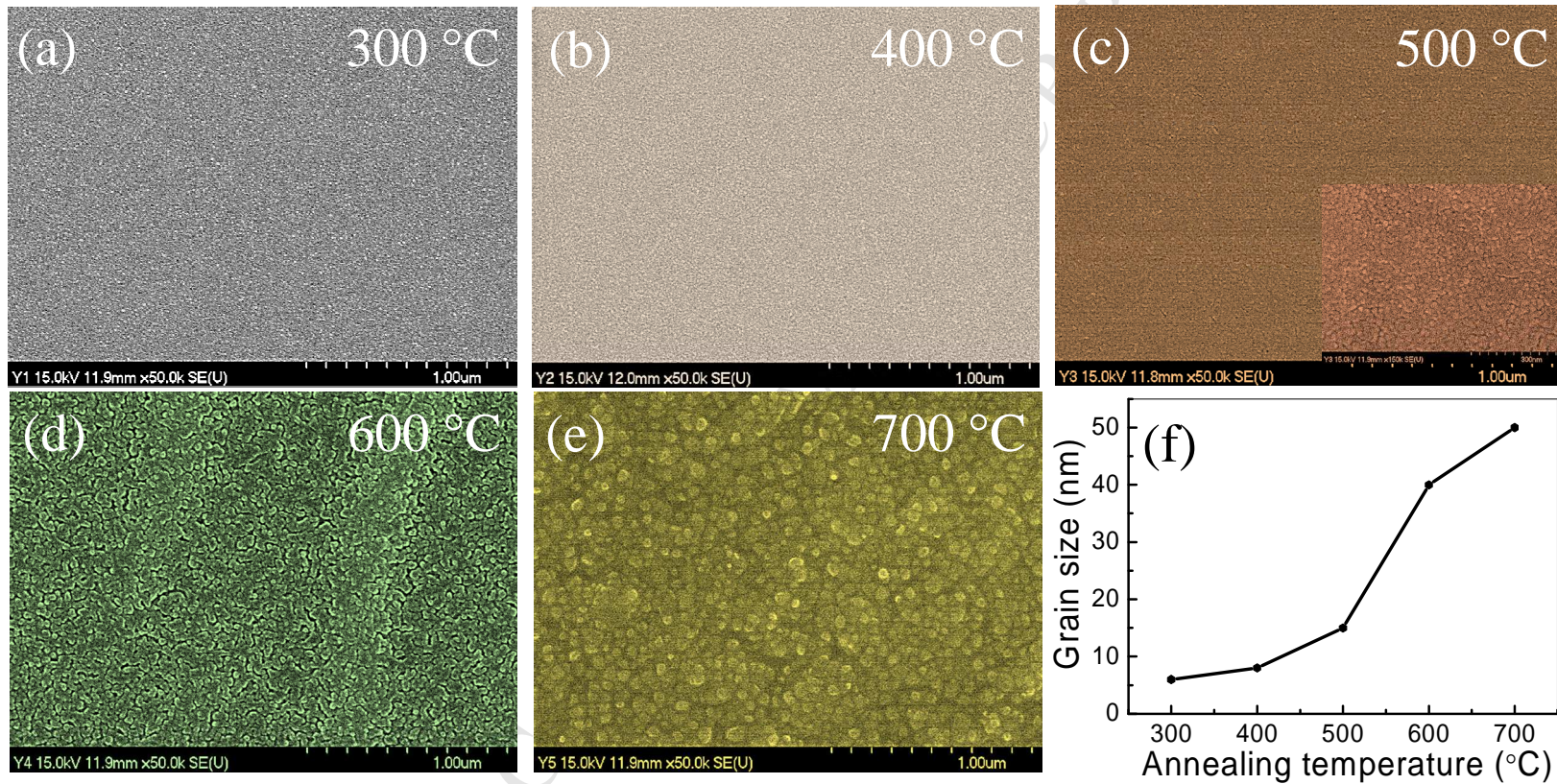
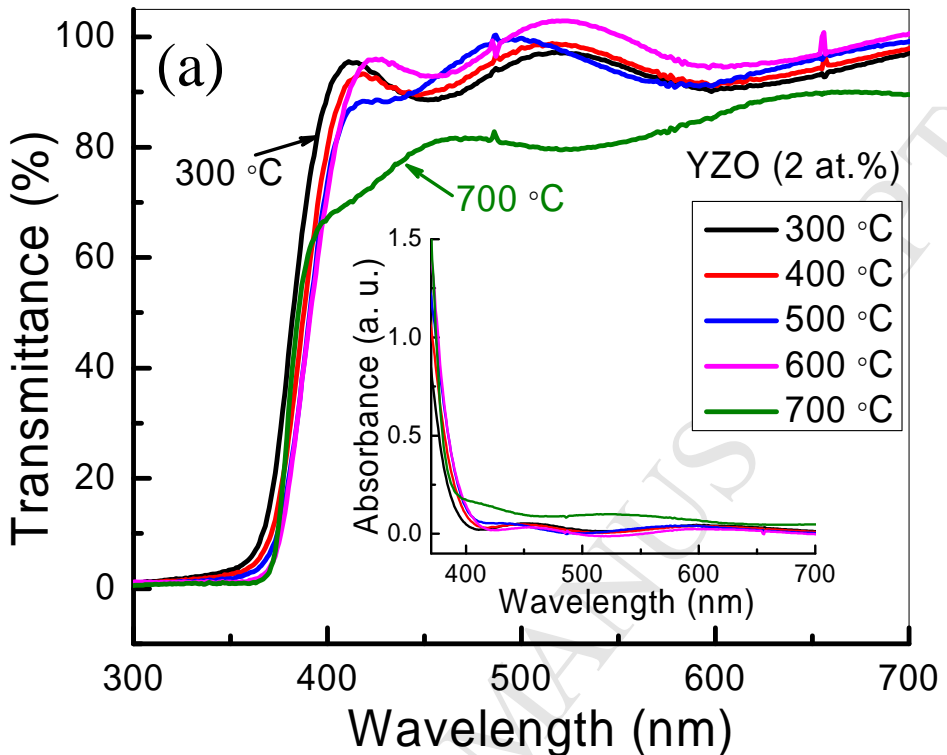
Fig. 2

Fig. 3

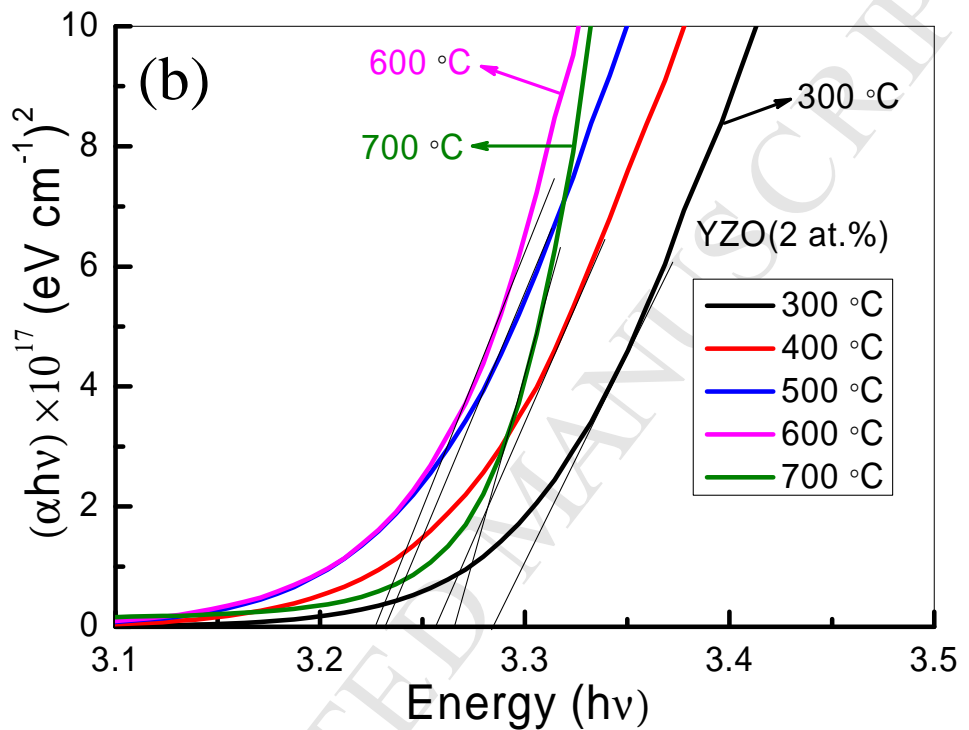


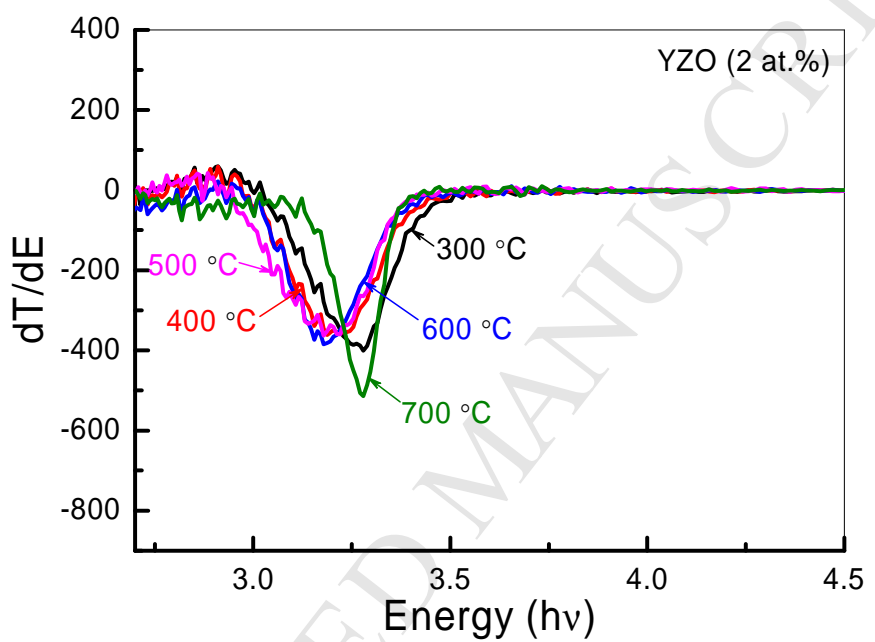
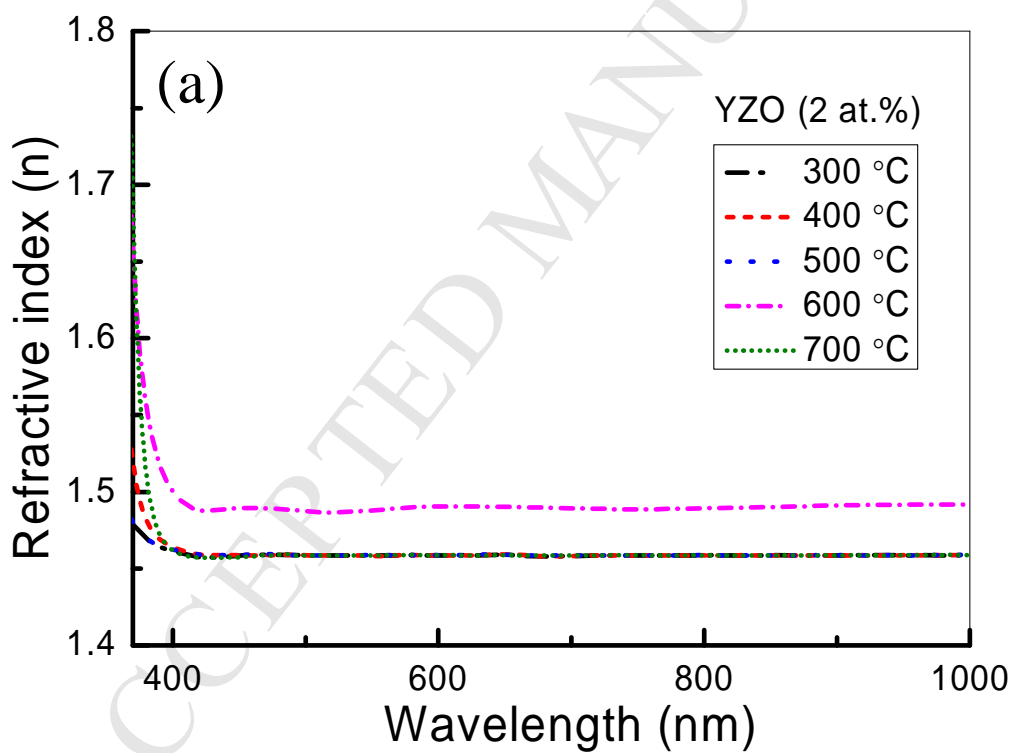
Fig. 4

Fig. 5

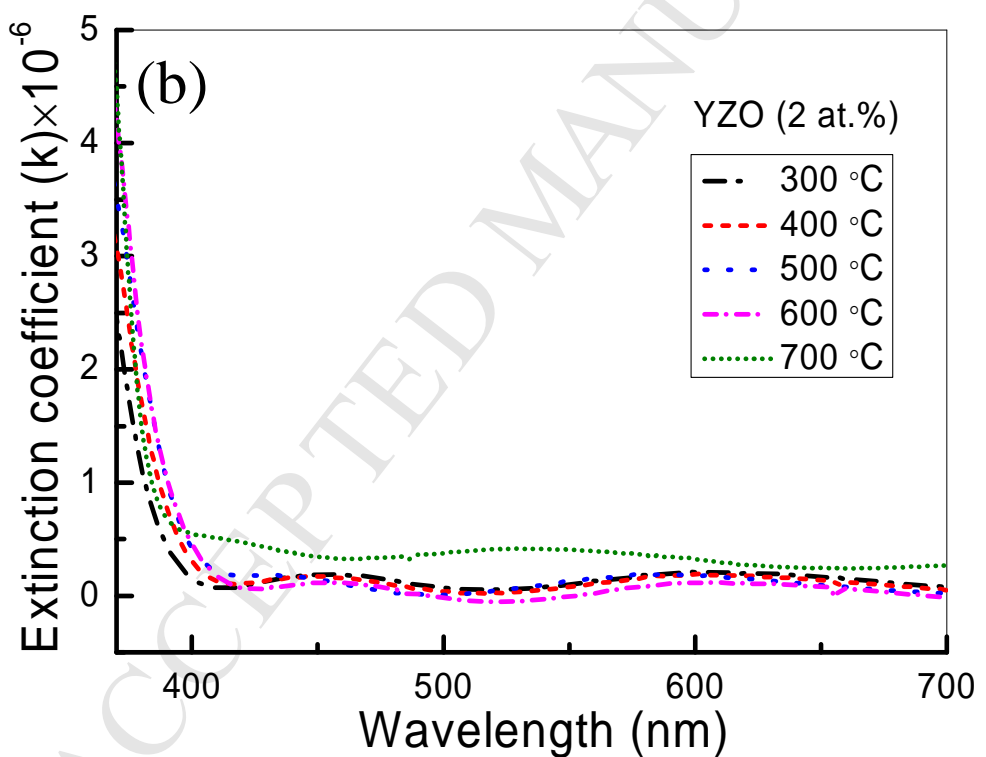


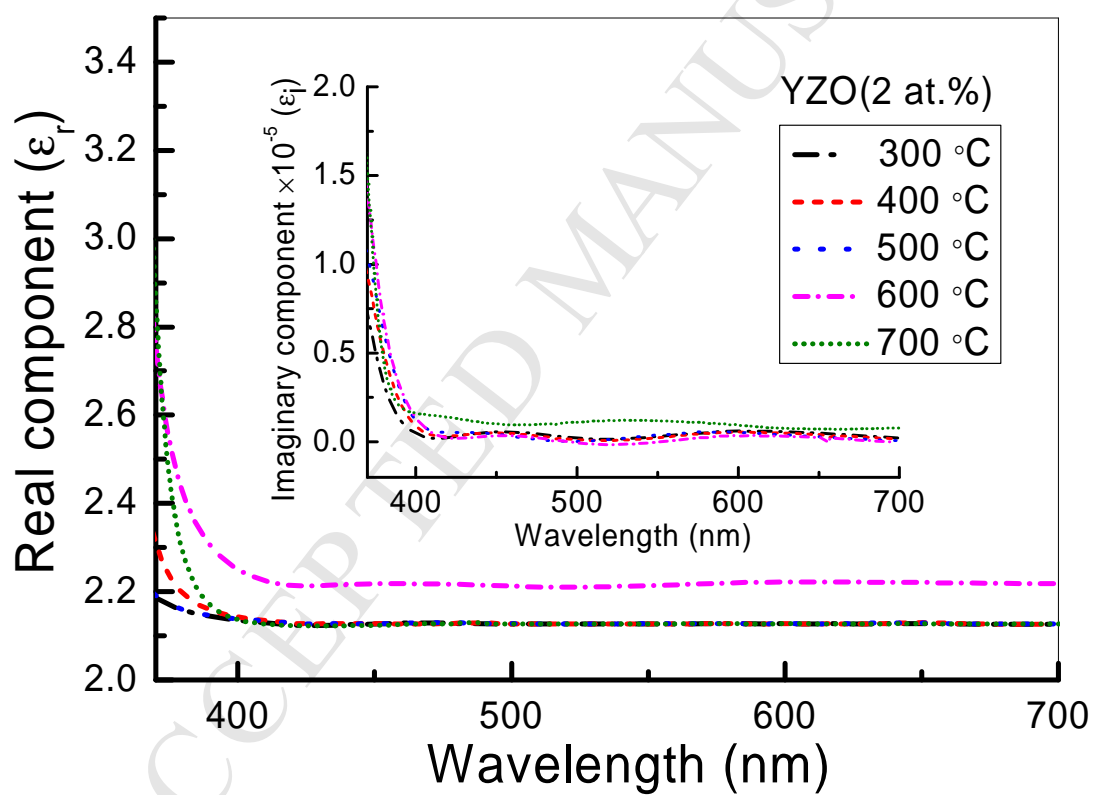
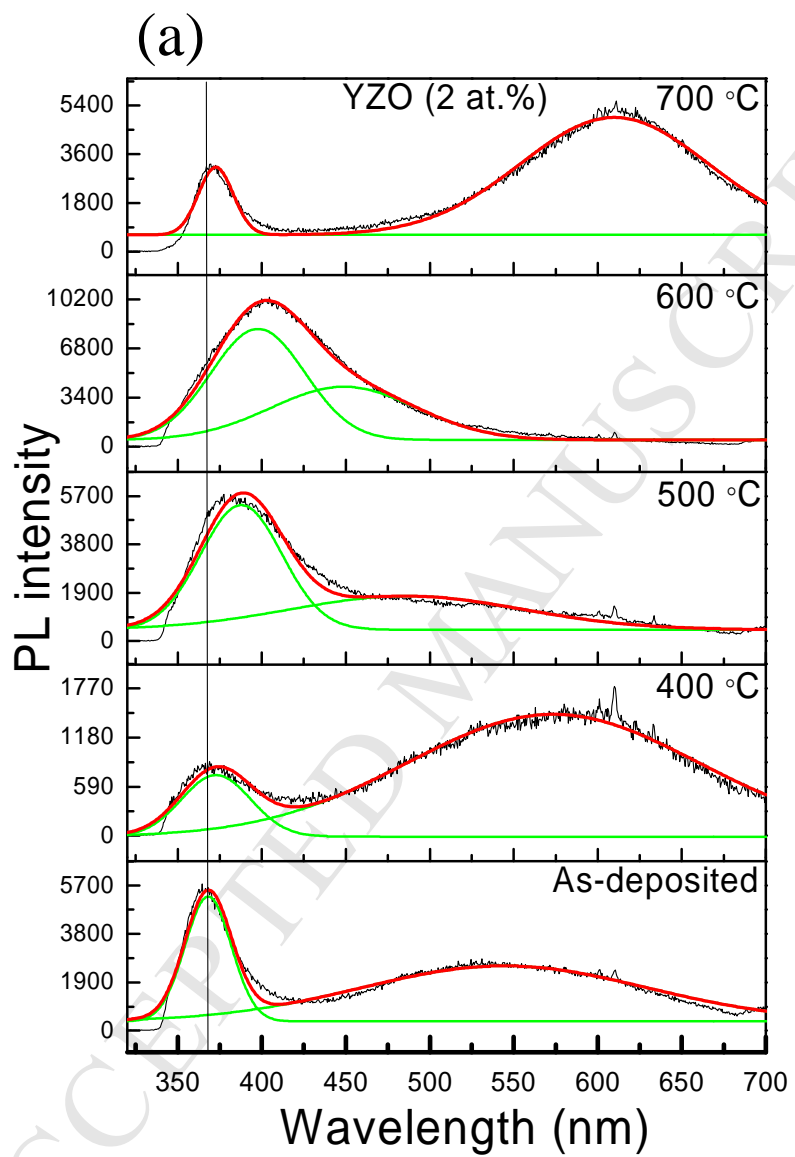
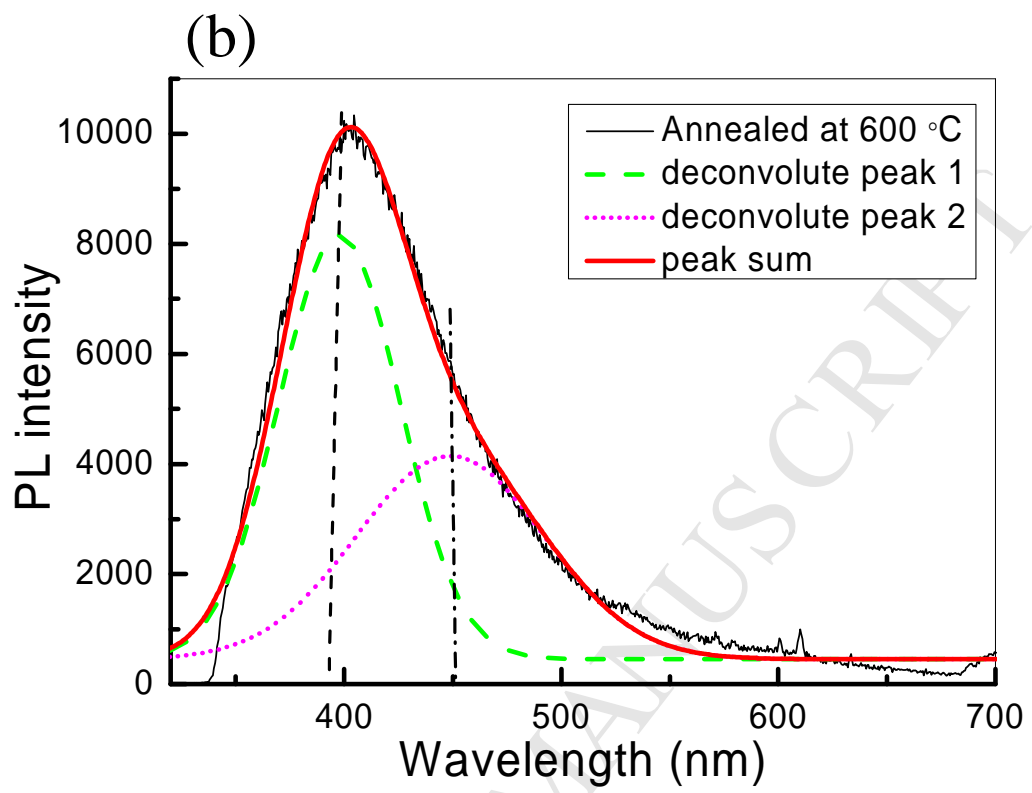
Fig. 6

Fig. 7



Highlights

1. YZO thin films were grown on quartz by the least expensive sol-gel method.
2. Vacuum annealing improved the crystallinity of YZO thin films.
3. Grain size of YZO films were found to be increased by annealing.
4. Stress relaxation were related to the tune of the bandgap in YZO thin films.
5. PL provides the evidence of shifting the bandgap owing to stress release phenomena.